

Instance by Instance: An Iterative Framework for Multi-instance 3D Registration

Xinyue Cao¹, Xiyu Zhang¹, Yuxin Cheng², Zhaoshuai Qi¹, Yanning Zhang¹, Jiaqi Yang^{1,*}

¹School of Computer Science, Northwestern Polytechnical University, China

²Department of Electronic and Computer Engineering, Chinese University of Hong Kong, China

¹{caoxinyue, 2426988253}@mail.nwpu.edu.cn; {zhaoshuaiqi1206, ynzhang, jqyang}@nwpu.edu.cn;

²yuxin.cheng@link.cuhk.edu.cn

Abstract

Multi-instance registration is a challenging problem in computer vision and robotics, where multiple instances of an object need to be registered in a standard coordinate system. In this work, we propose the first iterative framework called instance-by-instance (IBI) for multi-instance 3D registration (MI-3DReg). It successively registers all instances in a given scenario, starting from the easiest and progressing to more challenging ones. Throughout the iterative process, outliers are eliminated continuously, leading to an increasing inlier rate for the remaining and more challenging instances. Under the IBI framework, we further propose a sparse-to-dense-correspondence-based multi-instance registration method (IBI-S2DC) to achieve robust MI-3DReg. Experiments on the synthetic and real datasets have demonstrated the effectiveness of IBI and suggested the new state-of-the-art performance of IBI-S2DC, e.g., our MHFI is 12.02%/12.35% higher than the existing state-of-the-art method ECC on the synthetic/real datasets.

1. Introduction

Most research on 3D point cloud registration focuses on estimating a single transformation between pairwise point cloud [3, 4, 6, 8, 9, 17, 34, 40]. However, the target scene may contain multiple repeated instances in real applications, and the problem of estimating multiple transformations is called multi-instance 3D registration (MI-3DReg).

This task has been relatively underexplored. Early works [11, 14] use point pair features (PPF) to detect and estimate the pose transformations of the instances. The quality of correspondence has been enhanced with the emergence of deep-learned features, resulting in performance boosting for correspondence-based MI-3DReg [29, 38]. The first research on MI-3DReg based on correspondences is proposed in 2022 [29], *i.e.*, efficient corre-

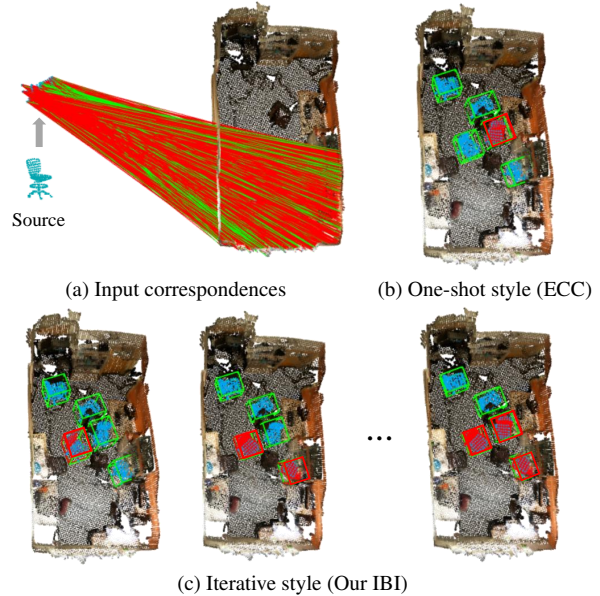


Figure 1. Comparison of one-shot method and our IBI for MI-3DReg. The inliers and outliers are visualized in green and red, respectively. The green and red bounding boxes represent the ground truth and estimated poses of instances, respectively.

spondence clustering (ECC), followed by a learned Point-CLM method [38]. Existing methods generally register all instances in a one-shot manner, demonstrating their efficiency. However, the correspondences between different instances can interfere with each other, making the registration of instances with low inlier rate very difficult.

To this end, we propose the first iterative framework called instance by instance (IBI) for robust MI-3DReg. We argue that inliers of a specific instance appear to be outliers to other instances. IBI iteratively registers instances and reduces outliers for each instance, which can effectively alleviate the registration problem for instances with scarce

inliers. First, a small set of highly consistent correspondences are selected as seed correspondences. Second, the seed correspondence set guides the enhancement of consistent correspondences to retrieve more inliers. Third, the six-degree-of-freedom (6-DoF) pose transformation is estimated with a guided sample consensus strategy. Finally, the generated registration hypothesis is globally validated, and the input correspondence set is updated by removing correspondences belonging to the current instance. Fig. 1 shows that IBI is able to register more instances than traditional one-shot methods.

The contributions are as follows:

- We propose IBI, the first iterative framework in MI-3DReg. It iteratively refines the registration results for each instance and gradually improves the precision and robustness of the registration process.
- Under the IBI framework, we introduce a sparse-to-dense-correspondence-based iterative method called IBI-S2DC. It mines consistent yet sparse seed correspondences to guide the retrieval of the whole inlier set. Its MHF1 is 12.02%/12.35% higher than the existing state-of-the-art method ECC [29] on the synthetic/real datasets.

2. Related Work

2.1. 3D Point Cloud Registration

Pairwise 3D point cloud registration. 3D point cloud registration is an essential task in computer vision and robotics, including feature extraction, outlier rejection, and pose estimation. For the first stage, recent advances have highlighted the effectiveness of learning-based features over hand-designed ones in certain benchmarks, such as 3DMatch [39] and SpinNet [1]. However, they still require robust outlier removal mechanisms. For the second stage, traditional outlier rejection methods are summarized by Yang *et al.* [36], including individual-based methods (*e.g.*, SS [36], NNSR [19], SI [13], CV [33]) and group-based methods (*e.g.*, RANSAC [12], ST[18], GC [7], 3DHV [30], GTM [27]). Other techniques, such as GORE [6] and PMC [23], reduce outliers through geometric consistency tests. Bai *et al.* [3] combined traditional methods and deep learning approaches to propose a two-stage network called PointDSC. For the third stage, traditional methods such as RANSAC and its variants [4, 12, 25, 34, 37] follow a hypothesis verification process to estimate the 6-DoF pose transformation. On the other hand, FGR [41] and TEASER [32] solve transformations directly from noisy correspondences using robust estimators.

Multi-instance 3D point cloud registration. Multi-instance 3D point cloud registration is a complex problem in computer vision and robotics, involving the alignment of multiple object instances in a shared coordinate system. To the best of our knowledge, there are only two existing

solutions for correspondence-based MI-3DReg. ECC [29] pioneers multi-instance point cloud registration by classifying initial correspondences into sets related to different instances, rejecting outliers, and resolving ambiguity. PointCLM [38], a contrastive-learning-based method, presents representation learning and outlier pruning strategies suitable for MI-3DReg. Overall, the research particularly for MI-3DReg is still at an early stage.

2.2. Multi-model Fitting

Theoretically, multi-model fitting methods can be also applied to MI-3DReg. Multi-model fitting methods estimate model parameters from data points generated by multiple models. Many existing methods perform one-shot model fitting. T-Linkage [20] initializes a broad hypothesis set through point sampling and clustering with preference vectors for outlier removal. RansaCov [21] addresses multi-model fitting as a maximum coverage problem, offering approximate solutions. Alternatively, some methods rely on sequential RANSAC-based fitting. Progressive-X [5] uses revised RANSAC with modified sampling weights to obtain distinct model parameters iteratively. CONSAC [16] incorporates deep models, akin to PointNet, for guiding the sampling process. However, they become inefficient when handling large-scale inputs.

Existing one-shot style MI-3DReg methods have overlooked the correspondence interference between instances, while multi-model fitting methods fail to incorporate proper point cloud geometric constraints. Motivated by these concerns, we propose a novel iterative IBI framework with two traits. First, it refines the registration results of each instance iteratively. Second, it enhances the registration accuracy and robustness progressively. It effectively alleviates the mutual interference issue caused by correspondences belonging to different instances, which is a common challenge encountered in one-shot methods.

3. The IBI Iterative Framework

3.1. Problem Formulation

For two point clouds \mathbf{P}^s and \mathbf{P}^t to be registered, \mathbf{P}^s represents the source instance and there are multiple instances of \mathbf{P}^s presented in \mathbf{P}^t . Let \mathbf{p}^s and \mathbf{p}^t respectively denote the points in the \mathbf{P}^s and \mathbf{P}^t , IBI estimates the 6-DoF pose transformations $\{\mathbf{R}_i, \mathbf{t}_i\}_{i=1,2,\dots,k}$ between the source instance in \mathbf{P}^s and multiple instances in \mathbf{P}^t , where k presents the number of repeated instances.

3.2. The Pipeline of IBI Framework

An initial correspondence set $\mathbf{C} = \{\mathbf{c}\}$ is served as input, where $\mathbf{c} = (\mathbf{p}^s, \mathbf{p}^t)$. It can be obtained by matching point cloud features. For dense input, we usually downsample the \mathbf{C} to $\mathbf{C}_{downsample}$, which contains $N_{downsample}$ cor-

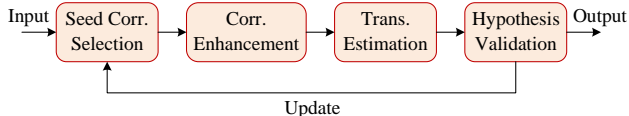


Figure 2. Schematic illustration of the IBI framework.

respondences. The IBI framework includes four steps, *i.e.*, seed correspondence selection (SCS), correspondence enhancement (CE), transformation estimation (TE), and hypothesis validation (HV). First, a set of sparse yet consistent seed correspondences is selected to identify a single consistency from $\mathbf{C}_{downsample}$. Second, the seed correspondences are utilized to guide the enhancement of consistent correspondences. Third, the pose transformation of a single instance is estimated by a robust 6-DoF estimator. Finally, the generated registration hypotheses are validated, where a correct hypothesis indicates the identification of a valid instance in the target point cloud. After validation, the correspondences related to the identified instance are removed and the iterative framework proceeds to the next instance. The registration framework is illustrated in Fig. 2.

4. A Trail on IBI for MI-3DReg

In this section, under the IBI framework, we propose IBI-S2DC for MI-3DReg, the pipeline is shown in Fig. 3.

4.1. SCS: Game-theoretic Matching

It is challenging to directly retrieve all inliers from the input because the scale is usually large and correspondences belonging to different instances exist simultaneously. To address this, we propose a sparse-to-dense-based mechanism. For sparse correspondences, we propose to mine a set of seed correspondences with high consistency under the game-theoretic matching (GTM) [38] guidance.

First, \mathbf{P}^s and \mathbf{P}^t are treated as a pair of players, and candidate correspondences in $\mathbf{C}_{downsample}$ are available strategies. The amount of population \mathbf{x} that plays each strategy \mathbf{c}_i at a given time is defined as:

$$\mathbf{x} = (\mathbf{x}_1, \dots, \mathbf{x}_{|\mathbf{C}_{downsample}|})^T. \quad (1)$$

Then we set the initial population around the barycenter, and then the population will dynamically update with an evolutionary process by applying the following replicator dynamics equation:

$$\mathbf{x}_i(t+1) = \mathbf{x}_i(t) \frac{(\Pi \mathbf{x}(t))_i}{\mathbf{x}(t)^T \Pi \mathbf{x}(t)}, \quad (2)$$

where Π is the payoff matrix that assigns the payoff between strategies \mathbf{c}_i and \mathbf{c}_j to row i and column j , and it is measured by the compatibility as:

$$\Pi = \begin{cases} r(\mathbf{c}_i, \mathbf{c}_j), & \text{if } \mathbf{c}_i \neq \mathbf{c}_j, \\ 0, & \text{otherwise} \end{cases}, \quad (3)$$

where the rigidity term $r(\mathbf{c}_i, \mathbf{c}_j)$ is:

$$r(\mathbf{c}_i, \mathbf{c}_j) = \left| \|\mathbf{p}_i - \mathbf{p}_j\| - \|\mathbf{p}'_i - \mathbf{p}'_j\| \right|. \quad (4)$$

The dynamics will converge to a Nash equilibrium [31]. After N_{gtm} times of evolution, the correspondences whose strategies are greater than a threshold t_{gtm} , are served as inliers. This step makes an efficient selection of the input correspondence set $\mathbf{C}_{downsample}$, generating a sparse correspondence set \mathbf{C}_s , which is highly consistent.

4.2. CE: Voting-based Enhancement

After SCS, the seed correspondence set is consistent but sparse, which cannot guarantee the accuracy of instance registration. Therefore, we propose a voting-based method, in order to retrieve more inliers from the input correspondence set. In particular, it calculates a voting score for each correspondence based on the consistency check between the input correspondences and the voting set. We propose to serve the seed correspondence set as the voting set to improve the voting reliability. The pipeline of consistency voting is illustrated in Fig. 4.

First, the sparse correspondences set \mathbf{C}_s is served as the voting set \mathbf{C}_{vot} . The correspondences in \mathbf{C}_s are voters and those in \mathbf{C} are candidates.

Second, we introduce a compatibility measure for a correspondence pair $(\mathbf{c}_i, \mathbf{c}_j)$ with single consistency:

$$D(\mathbf{c}_i, \mathbf{c}_j) = \exp\left(-\frac{r(\mathbf{c}_i, \mathbf{c}_j)^2}{\delta_r^2}\right), \quad (5)$$

where δ_r represents the rigidity parameters.

Third, all voters cast their votes for the candidates in the input correspondence set \mathbf{C} . The final voting score of a correspondence \mathbf{c} is defined as the sum of all compatibility scores of \mathbf{c} and $\mathbf{c}_i \in \mathbf{C}_{vot}$:

$$s(\mathbf{c}) = \sum_{\mathbf{c}_i \in \mathbf{C}_{vot}} D(\mathbf{c}, \mathbf{c}_i). \quad (6)$$

The correspondences are ranked based on voting scores in descending order, and the top N_{vot} correspondences are kept as inliers.

This step verifies and enhances the consistency of the sparse correspondence set \mathbf{C}_s , resulting in a dense correspondence set \mathbf{C}_d .

4.3. TE: Guided Sample Consensus

Single-instance 6-DoF pose transformation estimation is typically achieved with RANSAC [12]. However, the original RANSAC is sensitive to outliers and usually requires a

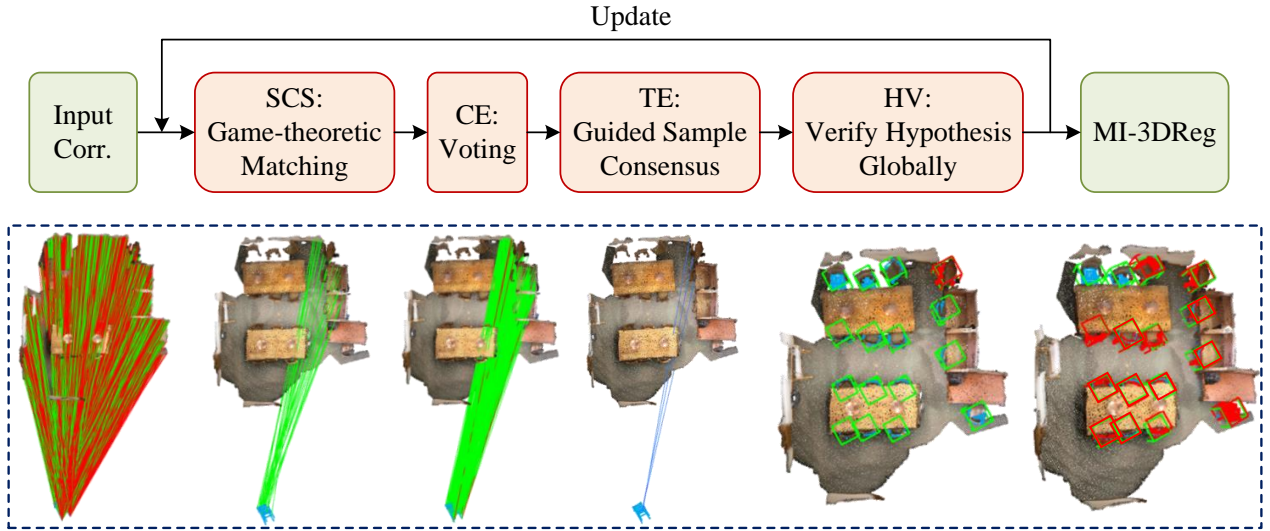


Figure 3. The pipeline of IBI-S2DC. 1. SCS: Mine a sparse yet consistent correspondence set C_s under GTM guidance. 2. CE: Enhance consistency to achieve a dense correspondence set C_d based on a voting scheme. 3. TE: Estimate the transformation for the current instance based on a guided sample consensus estimator (GSAC). 4. HV: Validate the hypothesis globally using the point cloud overlap rate.

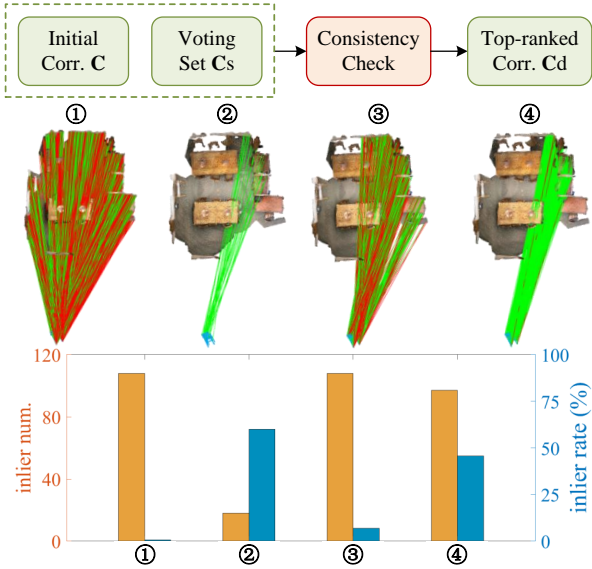


Figure 4. The pipeline of the voting-based correspondence enhancement. After mining a sparse correspondence set, the inlier rate of the instance rises but the number of inliers is very small. The voting-based enhancement helps to retrieve significantly more inliers while maintaining a high inlier rate, resulting in a consistent and dense correspondence set.

number of iterations. In our TE step, we propose a guided sampling consensus (GSAC) method to fully utilize the vot-

ing score constraints as sampling weight. It can improve the accuracy of transformation estimation and reduce the number of iterations.

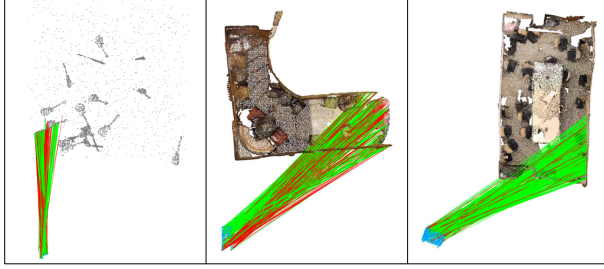
First, correspondence triplets are generated from C_d with three-point-sampling. Then, they are sorted in descending order based on the sum of the voting scores of the sampled three correspondences. After N_{gsac} iterations, the generated hypotheses are evaluated to identify the optimal hypothesis as the output of GSAC. Specifically, we use the mean absolute error (MAE) [35] to assess the quality of a hypothesis T_i . The MAE score is defined as:

$$S_{mae}(T_i) = \sum_{i=1}^{|C|} f(c_i), \quad (7)$$

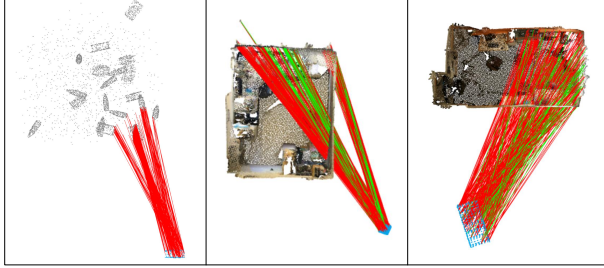
where the transformation error of c_i is defined as:

$$f(c_j) = \begin{cases} \frac{|e(c_i) - t_{he}|}{t_{he}}, & \text{if } e(c_i) < t_{he} \\ 0, & \text{otherwise} \end{cases}, \quad (8)$$

where $e(c_i) = \|\mathbf{R}_i \mathbf{p}_i^s + \mathbf{t}_i - \mathbf{p}_i^t\|$ represents the transformation error of c_i . In addition, t_{he} is a distance threshold to judge whether c_i is an inlier. The hypothesis with the highest MAE score is served as the final pose transformation for the current instance.



(a) Correspondences with high inlier rate yet multiple consistencies



(b) Correspondences with low inlier rate and multiple consistencies

Figure 5. In challenging registration cases, correspondences may still exhibit multiple consistencies and suffer from outliers after the CE step. In (a), the dense correspondences have a high inlier rate, while multiple-consistencies exist. In (b), there are multiple consistencies and many outliers in the dense correspondence set.

4.4. HV: Verify Hypothesis Globally

After the previous three steps, we perform post-validation for the transformation generated by TE. The motivation is that correspondences between the scene and the source model, even after the CE step, may still exhibit multi-consistency and suffer from outliers, as shown in Fig. 5. It is potentially due to that some instances are spatially very close, so the consistencies are hard to distinguish. This indicates that simply using correspondence-level information for hypothesis validation is not sufficient. Hence, we further propose a validation step that leverages global point-cloud-level information for hypothesis verification.

In particular, the overlap rate between two point clouds is considered for validation. First, we define the set of overlapped points as [26]:

$$\mathbf{P}_{op} = \{\mathbf{p}_i^{s'} | d(\mathbf{p}_i^{s'}, \mathbf{P}^t) \leq d_{op}^{th}, \mathbf{p}_i^{s'} \in \mathbf{P}^{s'}\}, \quad (9)$$

where $\mathbf{P}^{s'}$ represents the transformed point cloud, and the ‘point-to-surface’ distance $d(\mathbf{p}_i^{s'}, \mathbf{P}^t)$ is:

$$d(\mathbf{p}_i^{s'}, \mathbf{P}^t) = \min_{\mathbf{p}_j^t \in \mathbf{P}^t} \|\mathbf{p}_i^{s'} - \mathbf{p}_j^t\|, \quad (10)$$

where d_{op}^{th} is a distance threshold to determine if two points are in the overlapped area of \mathbf{P}^s and \mathbf{P}^t . Then we define the overlap rate as:

$$overlap = \frac{|\mathbf{P}_{op}|}{|\mathbf{P}^s|}, \quad (11)$$

Algorithm 1 IBI-S2DC Algorithms

Input: the point correspondences \mathbf{C}

Output: the 6-DoF pose transformations of target instances

- 1: Downsample \mathbf{C} to $\mathbf{C}_{downsample}$ with $N_{downsample}$ correspondences
 - 2: **while** the size of $N_s > t_s$ **do**
 - 3: Initial the payoff matrix $\Pi(i, j)$
 - 4: **for** $i = 0; i < N_{gtm}; i++$ **do**
 - 5: Compute the population $\mathbf{V}(j)$
 - 6: Update $\mathbf{V}(j)$ dynamically by Eq. 2
 - 7: **end for**
 - 8: Compute the sparse correspondence set \mathbf{C}_s
 - 9: **for** $j = 0; j < N_{vot}; j++$ **do**
 - 10: Compute consistency score by Eq. 5
 - 11: Compute voting score by Eq. 6
 - 12: Compute the dense correspondence set \mathbf{C}_d
 - 13: **end for**
 - 14: Rank \mathbf{C}_d by voting scores in descending order
 - 15: **for** $k = 0; k < N_{gsac}; k++$ **do**
 - 16: Perform guided three-point-sampling in \mathbf{C}_d
 - 17: Evaluate hypotheses with Eq. 7 and keep the best hypothesis
 - 18: **end for**
 - 19: Validate the kept hypothesis
 - 20: **if** $overlap > t_{overlap}$ **then**
 - 21: Serve the hypothesis as the predicted transformation
 - 22: Update the input correspondence set $\mathbf{C} \leftarrow \mathbf{C} - \mathbf{C}_d$
 - 23: **end if**
 - 24: **end while**
-

where $|\cdot|$ denotes the cardinality of a set.

If $overlap > t_{overlap}$, the hypothesis is accepted and an instance is supposed to be registered. Then its corresponding dense correspondence set \mathbf{C}_d is removed from the initial correspondence set. This helps on one hand reduce the input size and, on the other, improve the inlier ratio of the remaining instances. Otherwise, the iteration will switch to the SCS step. Note that we still remove \mathbf{C}_d when $overlap$ is smaller than $t_{overlap}$, to prevent the iteration from getting stuck in an endless loop. Because the number of instances in the 3D scene is unknown, an iteration stop criterion is required. We assume that when the number of sparse correspondences $N_s < t_s$, the consistency is not strong enough, and the iteration stops (see Algorithm 1 for pseudocode).

5. Experiment

5.1. Experimental Setup

Datasets. We conduct experiments on both synthetic and real datasets. The synthetic dataset is created based on pre-

Metrics	MHR(%)	MHP(%)	MHF1(%)	Times(s)
T-Linkage [20]	0.19	0.54	0.27	43.46
Prog-X [5]	15.90	31.01	18.98	86.39
CONSAC [16]	0.10	0.07	0.08	7.65
ECC [29]	53.39	61.44	51.80	1.28
PointCLM [38]	0.62	0.18	0.28	0.50
IBI-S2DC	61.16	71.20	63.82	6.28

Table 1. Results on the synthetic dataset.

sampling the ModelNet40 dataset using PointNet++ [24]. Each point cloud is downsampled to 256 points, and K (up to 20) random transformations mixed with other objects and random points are applied to form the target point cloud.

Scan2CAD [2] serves as a real benchmark dataset aligning ShapeNet [28] CAD models with object instances in ScanNet [10] point clouds. We sample pairs that contain multiple CAD models in scans for testing.

Metrics. We adopt the three metrics for MI-3DReg task proposed in ECC [29], including Mean Hit Recall (MHR), Mean Hit Precision (MHP), and Mean Hit F1 ($MHF1$).

Implementation details. We compare the proposed IBI-S2DC with five state-of-the-art methods for MI-3DReg: PointCLM (2022) [38], ECC (2022) [29], T-linkage (2014) [20], Progressive-X (2019) [5], and CONSAC (2020) [16]. For a fair comparison, all methods employ the same point correspondences as input. In PointCLM, we directly utilize the trained models in the synthetic and real datasets provided by the authors for evaluation.

The parameters of our method are set as follows: $N_{downsample} = 1024$, $N_{gtm} = 20$, and $N_{vot} = 300$. The threshold t_{gtm} is calculated by OSTU [22]. The term δ_r in the CE step is set to 10 pr. Here, ‘pr’ is the resolution of a point cloud [33]. Stop criteria t_s is set to 5. For the synthetic dataset, we set $N_{gsac} = 100$, $t_{he} = 10$ pr, $d_{op}^{th} = 1.5$ pr, and $t_{overlap} = 0.85$. For the real dataset, we set $N_{gsac} = 20$, $t_{he} = 1$ pr, $d_{op}^{th} = 3$ pr, and $t_{overlap} = 0.7$.

5.2. Comparative Experiments

5.2.1 Synthetic Dataset

We employ the correspondences generated by PREDATOR [15], as same as ECC [29]. Table 1 shows the performance on the synthetic dataset. The results demonstrate that even under challenging initial conditions with an outlier rate exceeding 90%, IBI-S2DC manages to perform admirably. The MHR is 61.16%, the MHP is 71.20%, and the MHF1 is 63.82%. Although IBI-S2DC trails slightly behind PointCLM and ECC in terms of efficiency, its performance remains far better than those of the two competitors. We present some visual results in Fig. 6.

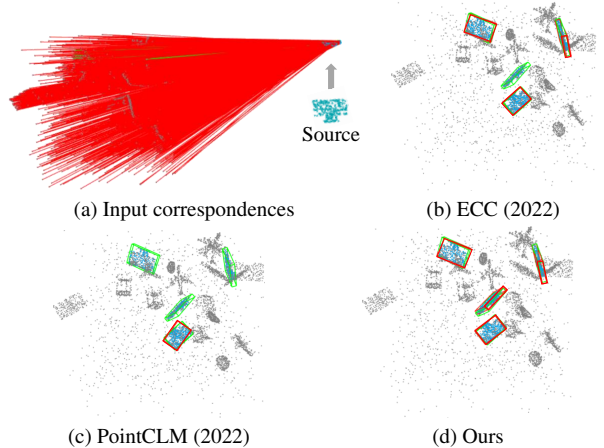


Figure 6. Results on the synthetic dataset. (a) displays the input correspondences. (b-d) show the results of several compared methods. Here, estimated poses and the ground truth ones are rendered in red and green bounding boxes, respectively.

Metrics	MHR(%)	MHP(%)	MHF1(%)	Times(s)
T-Linkage [20]	2.46	3.79	2.71	1655.00
Prog-X [5]	11.58	6.86	7.87	26.32
CONSAC [16]	2.66	0.35	0.62	21.35
ECC [29]	31.63	29.23	27.04	1.46
PointCLM [38]	1.78	0.73	1.04	0.19
IBI-S2DC	50.31	36.30	39.39	7.56

Table 2. Results on the real dataset.

5.2.2 Real Dataset

Table 2 reports the results on the real dataset. It indicates that for correspondence generated by PREDATOR [15] with an outlier rate exceeding 75%, IBI-S2DC consistently outperforms all competitors. The MHR is 50.31%, the MHP is 36.30%, and the MHF1 is 39.39%. This demonstrates the superiority of IBI-S2DC in large-scale and complex 3D real scenes. PointCLM, a deep-learned method, exhibits very limited performance when applied to the data setting by ECC. Fig. 7 provides visualizations of several results.

5.3. Analysis Experiments

5.3.1 Validation Globally or Locally

We find that after the CE step, there may still be multiple consistencies in C_d . Therefore, hypotheses need further validation. We compare the performance of validation globally (using point cloud overlap rate) and locally (using inlier count [35]) to demonstrate our statement, as shown in Table 3. Two observations can be made. 1) Without hypothesis validation (referring to the control group), IBI-S2DC ex-

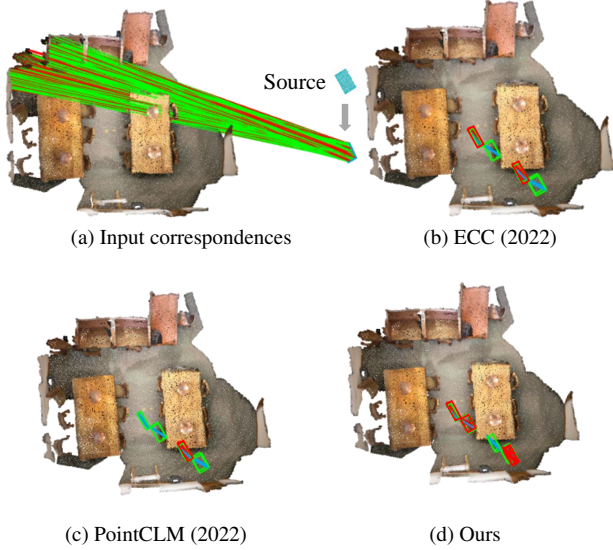


Figure 7. Results on the real dataset.

Metrics	MHR(%)	MHP(%)	MHF1(%)	Times(s)
Control group: without hypothesis validation, $N_s < t_s$				
$t_s = 5$	59.56	26.03	32.68	6.21
$t_s = 10$	54.90	26.46	32.03	6.03
$t_s = 15$	50.05	26.97	31.33	5.24
Experimental group: the inlier count, $\#inliers > t_{inliers}$				
$t_{inliers} = 50$	60.12	25.15	32.03	8.02
$t_{inliers} = 100$	51.25	25.69	30.56	7.60
$t_{inliers} = 150$	28.29	26.04	23.56	3.97
Experimental group: point cloud overlap rate, $overlap > t_{overlap}$				
$t_{overlap} = 0.8$	60.50	66.84	61.55	5.48
$t_{overlap} = 0.85$	61.16	71.20	63.82	6.28
$t_{overlap} = 0.9$	58.34	76.60	64.35	8.28

Table 3. The performance of IBI-S2DC with different hypothesis validation methods on the synthetic dataset.

hibits limited performance. 2) With global hypothesis validation, the result under different $t_{overlap}$ values consistently outperforms that with local hypothesis validation.

5.3.2 Robustness Analysis

Iterations of GTM. We analyze the impact of N_{gtm} in the SCS step, and set $N_{vot} = 300$ and $t_s = 5$. Fig. 8 shows the performance of our method under different N_{gtm} values. The results suggest that our method is very robust to N_{gtm} changes on the synthetic dataset. On the real dataset, the performance fluctuates slightly when N_{gtm} varies from 10 to 50. Overall, our method is robust to N_{gtm} variation.

Number of correspondences after voting. Here, we set

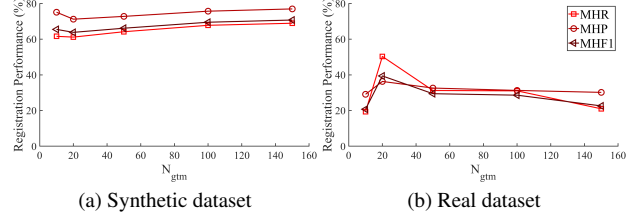


Figure 8. Robustness to N_{gtm} variation on the synthetic and real datasets.

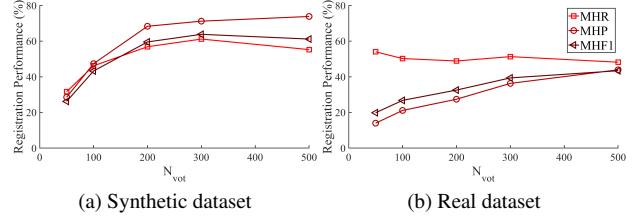


Figure 9. Robustness to N_{vot} variation on the synthetic and real datasets.

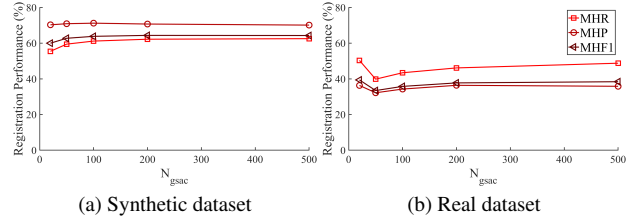


Figure 10. Robustness to N_{gsac} variation on the synthetic and real datasets.

$N_{gtm} = 20$, $t_s = 5$ and vary N_{vot} . Fig. 9 shows the performance of our method under different N_{vot} values. Generally, larger voting sets result in better performance. This indicates that more inliers are contained, while more consistency checks are required. When N_{vot} is greater than 200, the performance is very stable.

Iterations of GSAC. We set $N_{gtm} = 20$, $N_{vot} = 300$, $t_s = 5$, and vary N_{gsac} in this experiment. Fig. 10 shows the performance of our method under different N_{gsac} values. The results demonstrate that IBI-S2DC is robust to the N_{gsac} setting. Even with 20 iterations, we are able to achieve accurate 3D registration.

Varying correspondence densities. We examine the robustness of IBI-S2DC in the presence of inputs with various densities. Here, we set $N_{gtm} = 20$, $N_{vot} = 300$, $t_s = 5$, and N_{gsac} to 100 and 20 on the synthetic and real datasets, respectively. Table 4 and Table 5 report the results. On the synthetic dataset, our IBI-S2DC consistently outperforms ECC. In addition, we find that IBI-S2DC is quite stable when the number of input correspondences varies from 512 to 2048. When faced with extremely sparse input

Metrics		MHR(%)	MHP(%)	MHF1(%)	Times(s)
$N_{downsample}$					
256	ECC [29]	-	-	-	-
	IBI-S2DC	6.71	31.91	9.69	0.88
512	ECC [29]	48.78	62.92	51.26	0.32
	IBI-S2DC	59.66	72.25	63.42	6.11
1024	ECC [29]	53.39	61.44	51.80	1.28
	IBI-S2DC	61.16	71.20	63.82	6.28
2048	ECC [29]	53.98	59.37	50.41	2.05
	IBI-S2DC	54.91	72.92	60.32	6.61
5096	ECC [29]	-	-	-	-
	IBI-S2DC	47.23	71.52	54.14	8.62

Table 4. Performance with different $N_{downsample}$ values on the synthetic dataset. The term ‘-’ represents that it fails to get results under the tested scenario.

Metrics		MHR(%)	MHP(%)	MHF1(%)	Times(s)
$N_{downsample}$					
256	ECC [29]	32.11	28.70	28.40	0.32
	IBI-S2DC	37.36	36.67	32.43	3.58
512	ECC [29]	32.18	29.11	27.57	0.61
	IBI-S2DC	44.76	33.70	35.98	4.24
1024	ECC [29]	31.63	29.23	27.04	1.46
	IBI-S2DC	50.31	36.30	39.39	7.56
2048	ECC [29]	-	-	-	-
	IBI-S2DC	50.91	37.31	40.50	6.99
5096	ECC [29]	-	-	-	-
	IBI-S2DC	50.82	37.60	40.30	9.26

Table 5. Performance with different $N_{downsample}$ values on the real dataset.

(the correspondence count is smaller than 512), IBI-S2DC also yields limited performance. On the real dataset, IBI-S2DC consistently exhibits superior performance. Meanwhile, IBI-S2DC also achieves good performance with 256 input correspondences on the real dataset. These results indicate that IBI-S2DC possesses strong robustness to varying correspondence densities.

5.3.3 Module Effectiveness Analysis

Table 6 and Table 7 present the effectiveness analysis on the four modules of our IBI method, *i.e.*, SCS, CE, TE, and HV, on the synthetic and real datasets.

First, we analyze the SCS module. We remove the SCS module and replace the voting set in CE with the top-ranked correspondences sorted by nearest neighbor similarity ratio (NNSR) [19]. Without SCS, the MHF1 of IBI-S2DC decreases 52.32% and 10.85% on the synthetic and real datasets, respectively. This verifies the necessity of mining consistency with a sparse set. 3D Hough voting [30] is

SCS	CE	TE	HV	MHR(%)	MHP(%)	MHF1(%)	Times(s)
N				35.76	7.50	11.50	7.56
H				44.26	72.62	52.51	66.65
	✗			25.50	34.02	26.53	0.38
		R		54.25	<u>72.61</u>	59.69	<u>0.63</u>
		S		57.07	70.13	<u>60.68</u>	304.75
		M		57.56	68.13	60.00	12.04
			✗	<u>60.44</u>	25.70	32.51	6.35
			L	49.57	69.30	54.32	7.51
✓	✓	✓	✓	61.16	71.20	63.82	6.28

Table 6. Module effectiveness analysis on the synthetic dataset. ‘N’ represents NNSR, ‘H’ represents 3D Hough Voting [30], ‘R’ represents RANSAC[12], ‘S’ represents SAC-COT [34], ‘M’ represents MAC [40] and ‘L’ represents validate locally [35].

conducted as an alternative method.

Second, we ablate the CE module. We set the population of C_s as the guided sampling score for GSAC. Applying CE achieves MHF1 improvements of 37.29% and 21.77% on the synthetic and real datasets, respectively. This demonstrates that the CE module is critical to retrieving inliers and achieving accurate registration.

Third, we analyze the TE module. We replace GSAC with RANSAC, SACCOT, and MAC. Compared to GSAC, other solvers boost efficiency notably but meet a clear performance deterioration. This suggests that GSAC fully leverages the consistency information of the SCS and CE modules and effectively improves registration accuracy.

Fourth, we remove the HV module. Without hypothesis validation, the MHF1 results on the synthetic and real datasets drop by 31.31% and 23.45%, respectively. Local validation in the real dataset achieves better performance.

Finally, *we have also demonstrated that IBI is a general framework*. For instance, when employing RANSAC in the TE step, it achieves 59.69% in terms of MHF1, with a reduced time consumption at 0.63 seconds. This variant of IBI still surpasses ECC, demonstrating the flexibility of IBI. We believe the performance of IBI can be further improved with more advanced methods for each module.

6. Conclusion

In this paper, we presented an IBI framework for MI-3DReg by registering instances and reducing outliers iteratively. Under the framework, we further proposed IBI-S2DC and achieved state-of-the-art performance on all tested datasets. In particular, its MHF1 values are 12.02%/12.35% higher than the existing state-of-the-art method ECC on the synthetic/real datasets. We expect more trials under the proposed IBI framework in the future.

SCS	CE	TE	HV	MHR(%)	MHP(%)	MHF1(%)	Times(s)
N				34.47	28.92	28.55	6.41
H				33.18	31.02	29.69	46.23
	X			35.31	15.41	17.62	0.30
		R		29.30	28.28	26.17	<u>0.52</u>
		S		<u>57.73</u>	36.14	<u>41.28</u>	291.53
		M		60.05	34.36	40.28	22.46
			X	28.04	12.58	15.94	3.80
			L	52.59	51.72	48.54	6.47
✓	✓	✓	✓	50.31	<u>36.30</u>	39.39	7.56

Table 7. Module effectiveness analysis on the real dataset.

References

- [1] Sheng Ao, Qingyong Hu, Bo Yang, Andrew Markham, and Yulan Guo. Spinnet: Learning a general surface descriptor for 3d point cloud registration. In *Proc. of the IEEE/CVF Conference on Computer Vision and Pattern Recognition*, pages 11753–11762, 2021. **2**
- [2] Armen Avetisyan, Manuel Dahnert, Angela Dai, Manolis Savva, Angel X. Chang, and Matthias Nießner. Scan2cad: Learning cad model alignment in rgb-d scans. In *Proc. of the IEEE/CVF Conference on Computer Vision and Pattern Recognition*, pages 2609–2618, 2019. **6**
- [3] Xuyang Bai, Zixin Luo, Lei Zhou, Hongkai Chen, Lei Li, Zeyu Hu, Hongbo Fu, and Chiew-Lan Tai. Pointdsc: Robust point cloud registration using deep spatial consistency. In *Proc. of the IEEE/CVF Conference on Computer Vision and Pattern Recognition*, pages 15859–15869, 2021. **1, 2**
- [4] Daniel Barath and Jiří Matas. Graph-cut ransac. In *Proc. of the IEEE Conference on Computer Vision and Pattern Recognition*, pages 6733–6741, 2018. **1, 2**
- [5] Daniel Barath and Jiri Matas. Progressive-x: Efficient, anytime, multi-model fitting algorithm. In *Proc. of the IEEE/CVF International Conference on Computer Vision*, pages 3780–3788, 2019. **2, 6**
- [6] Alvaro Parra Bustos and Tat-Jun Chin. Guaranteed outlier removal for point cloud registration with correspondences. *IEEE Transactions on Pattern Analysis and Machine Intelligence*, 40(12):2868–2882, 2017. **1, 2**
- [7] Hui Chen and Bir Bhanu. 3d free-form object recognition in range images using local surface patches. *Pattern Recognition Letters*, 28(10):1252–1262, 2007. **2**
- [8] Zhi Chen, Kun Sun, Fan Yang, and Wenbing Tao. Sc2-pcr: A second order spatial compatibility for efficient and robust point cloud registration. In *Proc. of the IEEE/CVF Conference on Computer Vision and Pattern Recognition*, pages 13221–13231, 2022. **1**
- [9] Christopher Choy, Wei Dong, and Vladlen Koltun. Deep global registration. In *Proc. of the IEEE/CVF Conference on Computer Vision and Pattern Recognition*, pages 2514–2523, 2020. **1**
- [10] Angela Dai, Angel X. Chang, Manolis Savva, Maciej Halber, Thomas Funkhouser, and Matthias Nießner. Scannet: Richly-annotated 3d reconstructions of indoor scenes. In *Proc. of the IEEE Conference on Computer Vision and Pattern Recognition*, pages 2432–2443, 2017. **6**
- [11] Bertram Drost, Markus Ulrich, Nassir Navab, and Slobodan Ilic. Model globally, match locally: Efficient and robust 3d object recognition. In *IEEE Computer Society Conference on Computer Vision and Pattern Recognition*, pages 998–1005. IEEE, 2010. **1**
- [12] Martin A Fischler and Robert C Bolles. Random sample consensus: a paradigm for model fitting with applications to image analysis and automated cartography. *Communications of the ACM*, 24(6):381–395, 1981. **2, 3, 8**
- [13] Anders Glent Buch, Yang Yang, Norbert Kruger, and Henrik Gordon Petersen. In search of inliers: 3d correspondence by local and global voting. In *Proc. of the IEEE Conference on Computer Vision and Pattern Recognition*, pages 2067–2074, 2014. **2**
- [14] Jianwei Guo, Xuejun Xing, Weize Quan, Dong-Ming Yan, Qingyi Gu, Yang Liu, and Xiaopeng Zhang. Efficient center voting for object detection and 6d pose estimation in 3d point cloud. *IEEE Transactions on Image Processing*, 30:5072–5084, 2021. **1**
- [15] Shengyu Huang, Zan Gojcic, Mikhail Usvyatsov, Andreas Wieser, and Konrad Schindler. Predator: Registration of 3d point clouds with low overlap. In *Proc. of the IEEE/CVF Conference on Computer Vision and Pattern Recognition*, pages 4267–4276, 2021. **6, 1**
- [16] Florian Kluger, Eric Brachmann, Hanno Ackermann, Carsten Rother, Michael Ying Yang, and Bodo Rosenhahn. Consac: Robust multi-model fitting by conditional sample consensus. In *Proc. of the IEEE/CVF Conference on Computer Vision and Pattern Recognition*, pages 4634–4643, 2020. **2, 6**
- [17] Junha Lee, Seungwook Kim, Minsu Cho, and Jaesik Park. Deep hough voting for robust global registration. In *Proc. of the IEEE/CVF International Conference on Computer Vision*, pages 15994–16003, 2021. **1**
- [18] Marius Leordeanu and Martial Hebert. A spectral technique for correspondence problems using pairwise constraints. In *Proc. International Conference on Computer Vision*, pages 1482–1489. IEEE, 2005. **2**
- [19] David G Lowe. Distinctive image features from scale-invariant keypoints. *International Journal of Computer Vision*, 60:91–110, 2004. **2, 8**
- [20] Luca Magri and Andrea Fusiello. T-linkage: A continuous relaxation of j-linkage for multi-model fitting. In *Proc. of the IEEE Conference on Computer Vision and Pattern Recognition*, pages 3954–3961, 2014. **2, 6**
- [21] Luca Magri and Andrea Fusiello. Multiple model fitting as a set coverage problem. In *Proc. of the IEEE Conference on Computer Vision and Pattern Recognition*, pages 3318–3326, 2016. **2**
- [22] Nobuyuki Otsu. A threshold selection method from gray-level histograms. *IEEE Transactions on Systems, Man, and Cybernetics*, 9(1):62–66, 1979. **6**
- [23] Alvaro Parra, Tat-Jun Chin, Frank Neumann, Tobias Friedrich, and Maximilian Katzmann. A practical maximum clique algorithm for matching with pairwise constraints. *arXiv preprint arXiv:1902.01534*, 2019. **2**

- [24] Charles Ruizhongtai Qi, Li Yi, Hao Su, and Leonidas J Guibas. Pointnet++: Deep hierarchical feature learning on point sets in a metric space. *Advances in Neural Information Processing Systems*, 30, 2017. 6
- [25] Siwen Quan and Jiaqi Yang. Compatibility-guided sampling consensus for 3-d point cloud registration. *IEEE Transactions on Geoscience and Remote Sensing*, 58(10):7380–7392, 2020. 2
- [26] Siwen Quan, Jie Ma, Fangyu Hu, Bin Fang, and Tao Ma. Local voxelized structure for 3d binary feature representation and robust registration of point clouds from low-cost sensors. *Information Sciences*, 444:153–171, 2018. 5
- [27] Emanuele Rodolà, Andrea Albarelli, Filippo Bergamasco, and Andrea Torsello. A scale independent selection process for 3d object recognition in cluttered scenes. *International Journal of Computer Vision*, 102:129–145, 2013. 2
- [28] Manolis Savva, Fisher Yu, Hao Su, M Aono, B Chen, D Cohen-Or, W Deng, Hang Su, Song Bai, Xiang Bai, et al. Shrec16 track: largescale 3d shape retrieval from shapenet core55. In *Proc. of the Eurographics Workshop on 3D Object Retrieval*, 2016. 6
- [29] Weixuan Tang and Danping Zou. Multi-instance point cloud registration by efficient correspondence clustering. In *Proc. of the IEEE/CVF Conference on Computer Vision and Pattern Recognition*, pages 6667–6676, 2022. 1, 2, 6, 8
- [30] Federico Tombari and Luigi Di Stefano. Object recognition in 3d scenes with occlusions and clutter by hough voting. In *Pacific-Rim Symposium on Image and Video Technology*, pages 349–355. IEEE, 2010. 2, 8
- [31] Jörgen W Weibull. *Evolutionary game theory*. MIT press, 1997. 3
- [32] Heng Yang, Jingnan Shi, and Luca Carlone. Teaser: Fast and certifiable point cloud registration. *IEEE Transactions on Robotics*, 37(2):314–333, 2020. 2
- [33] Jiaqi Yang, Yang Xiao, Zhiguo Cao, and Weidong Yang. Ranking 3d feature correspondences via consistency voting. *Pattern Recognition Letters*, 117:1–8, 2019. 2, 6
- [34] Jiaqi Yang, Zhiqiang Huang, Siwen Quan, Zhaoshuai Qi, and Yanning Zhang. Sac-cot: Sample consensus by sampling compatibility triangles in graphs for 3-d point cloud registration. *IEEE Transactions on Geoscience and Remote Sensing*, 60:1–15, 2021. 1, 2, 8
- [35] Jiaqi Yang, Zhiqiang Huang, Siwen Quan, Qian Zhang, Yanning Zhang, and Zhiguo Cao. Toward efficient and robust metrics for ransac hypotheses and 3d rigid registration. *IEEE Transactions on Circuits and Systems for Video Technology*, 32(2):893–906, 2021. 4, 6, 8
- [36] Jiaqi Yang, Ke Xian, Peng Wang, and Yanning Zhang. A performance evaluation of correspondence grouping methods for 3d rigid data matching. *IEEE Transactions on Pattern Analysis and Machine Intelligence*, 43(6):1859–1874, 2021. 2
- [37] Jiaqi Yang, Jiahao Chen, Siwen Quan, Wei Wang, and Yanning Zhang. Correspondence selection with loose-tight geometric voting for 3-d point cloud registration. *IEEE Transactions on Geoscience and Remote Sensing*, 60:1–14, 2022. 2
- [38] Mingzhi Yuan, Zhihao Li, Qiuye Jin, Xinrong Chen, and Manning Wang. Pointclm: A contrastive learning-based framework for multi-instance point cloud registration. In *Proc. of the European Conference on Computer Vision*, pages 595–611. Springer, 2022. 1, 2, 3, 6
- [39] Andy Zeng, Shuran Song, Matthias Nießner, Matthew Fisher, Jianxiong Xiao, and Thomas Funkhouser. 3dmatch: Learning local geometric descriptors from rgb-d reconstructions. In *Proc. of the IEEE Conference on Computer Vision and Pattern Recognition*, pages 1802–1811, 2017. 2
- [40] Xiyu Zhang, Jiaqi Yang, Shikun Zhang, and Yanning Zhang. 3d registration with maximal cliques. In *Proc. of the IEEE/CVF Conference on Computer Vision and Pattern Recognition*, pages 17745–17754, 2023. 1, 8
- [41] Qian-Yi Zhou, Jaesik Park, and Vladlen Koltun. Fast global registration. In *Proc. of the European Conference on Computer Vision*, pages 766–782. Springer, 2016. 2

7. Performance with Varying Outlier Ratios

In this section, we create input correspondences by mixing GT correspondences with outliers instead of generating correspondences by PREDATOR [15], in order to control the outlier ratio *Outlier_ratio*. Various outlier ratios were examined, including 10% ~ 50%, 50% ~ 70%, and 70% ~ 90%. Outliers were randomly selected within specified ranges for each test instance. For parameters, we set $N_{gtm} = 20$, $N_{vot} = 300$, $N_{gsac} = 100$, and $t_{select} = 5$. The outcomes are detailed in Table 8. Our IBI-S2DC achieves notable and stable performance under each range of *Outlier_ratio*, and its MHF1 surpasses 90% under 10% ~ 90% outlier ratio. Our MHF1 also achieves 88.51% when facing extreme situations, *i.e.*, the outlier ratio exceeds 90%. This clearly indicates the robustness of our IBI-S2DC to varying outlier ratios.

Metrics	MHR(%)	MHP(%)	MHF1(%)	Times(s)	
<i>Outlier_ratio</i>					
10% ~ 50%	ECC [29]	21.72	61.90	29.70	1.58
	IBI-S2DC	97.74	88.10	92.36	2.85
50% ~ 70%	ECC [29]	21.01	53.49	27.87	2.22
	IBI-S2DC	98.41	85.79	91.30	4.04
70% ~ 90%	ECC [29]	20.65	33.41	22.99	2.60
	IBI-S2DC	98.49	84.05	90.25	5.39
90% ~ 99%	ECC [29]	-	-	-	-
	IBI-S2DC	99.10	80.94	88.51	13.62

Table 8. Performance with different *Outlier_ratio* values on the synthetic dataset.

8. Comparison with Correspondence-free Methods

Although our main focus is on correspondence-based methods for MI-3DReg, there are also some correspondence-free methods, typically including point-pair-feature-based (PPF) ones. Here, two PPF methods for comparison, including Drost_PPF [11] and Central_Voting_PPF [14]. Table 9 and Table 10 present the comparative results. Clearly, both PPF methods achieve very limited performance, and our IBI-S2DC achieves the best performance. This is because stable PPFs usually rely on dense and high-quality point clouds, while the datasets used for MI-3DReg are sparse and noisy.

Metrics	MHR(%)	MHP(%)	MHF1(%)	Times(s)
Drost_PPF [11]	7.52	5.45	5.34	2.20
Central_Voting_PPF [14]	3.61	3.78	3.15	5.68
IBI-S2DC	61.16	71.20	63.82	6.28

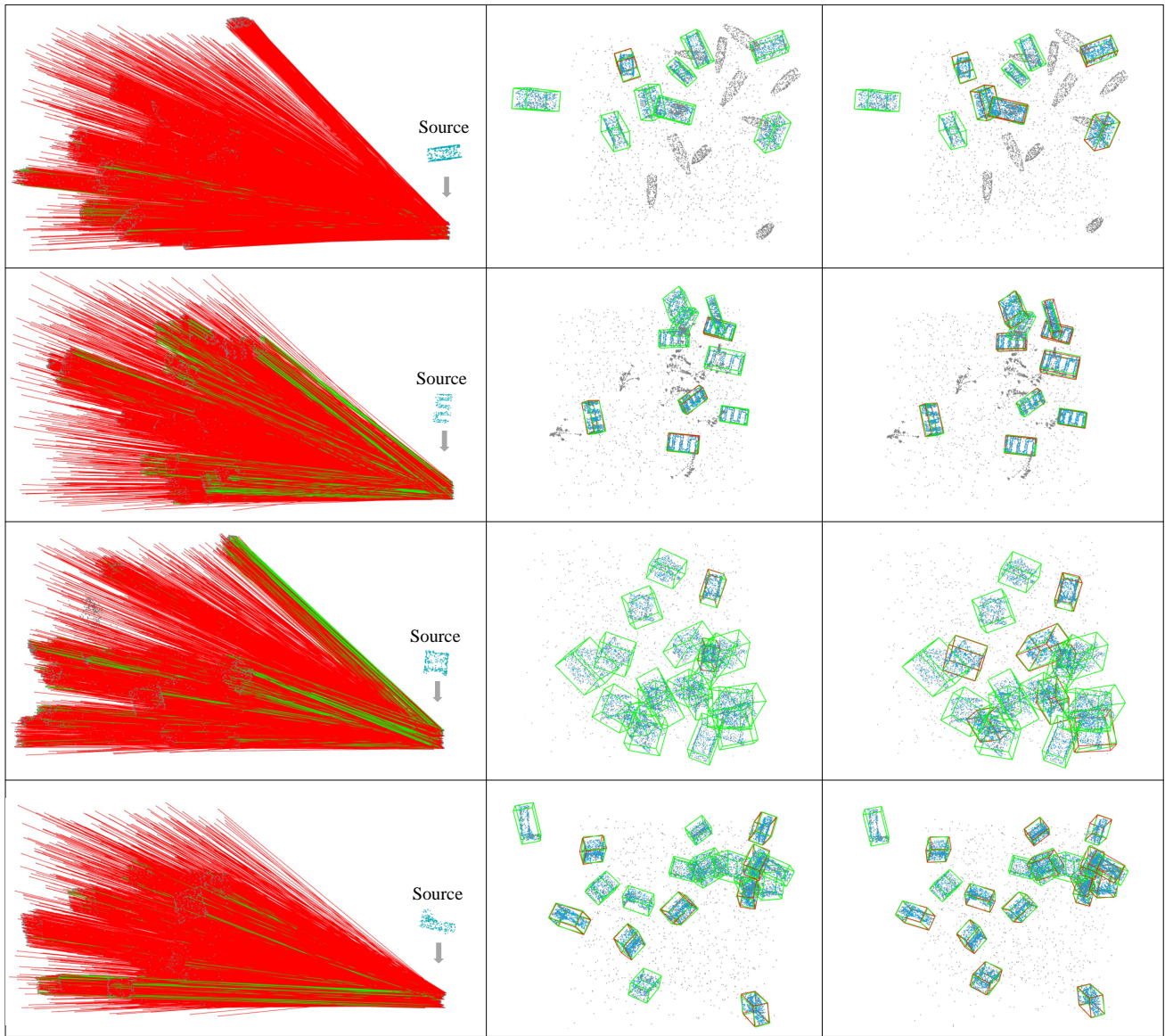
Table 9. Comparison with PPF methods on the synthetic dataset.

Metrics	MHR(%)	MHP(%)	MHF1(%)	Times(s)
Drost_PPF [11]	1.70	1.64	1.64	2.64
Central_Voting_PPF [14]	0.45	0.40	0.40	1.14
IBI-S2DC	50.31	36.30	39.39	7.56

Table 10. Comparison with PPF methods on the real dataset.

9. More Visualizations

More visualizations on the synthetic and real datasets are shown in Fig. 11 and Fig. 12, respectively. We compare with ECC and find that our IBI-S2DC successfully registers more instances in the presence of heavy outliers.



(a) Input correspondences

(b) ECC

(c) Ours

Figure 11. Visual results on the synthetic dataset.

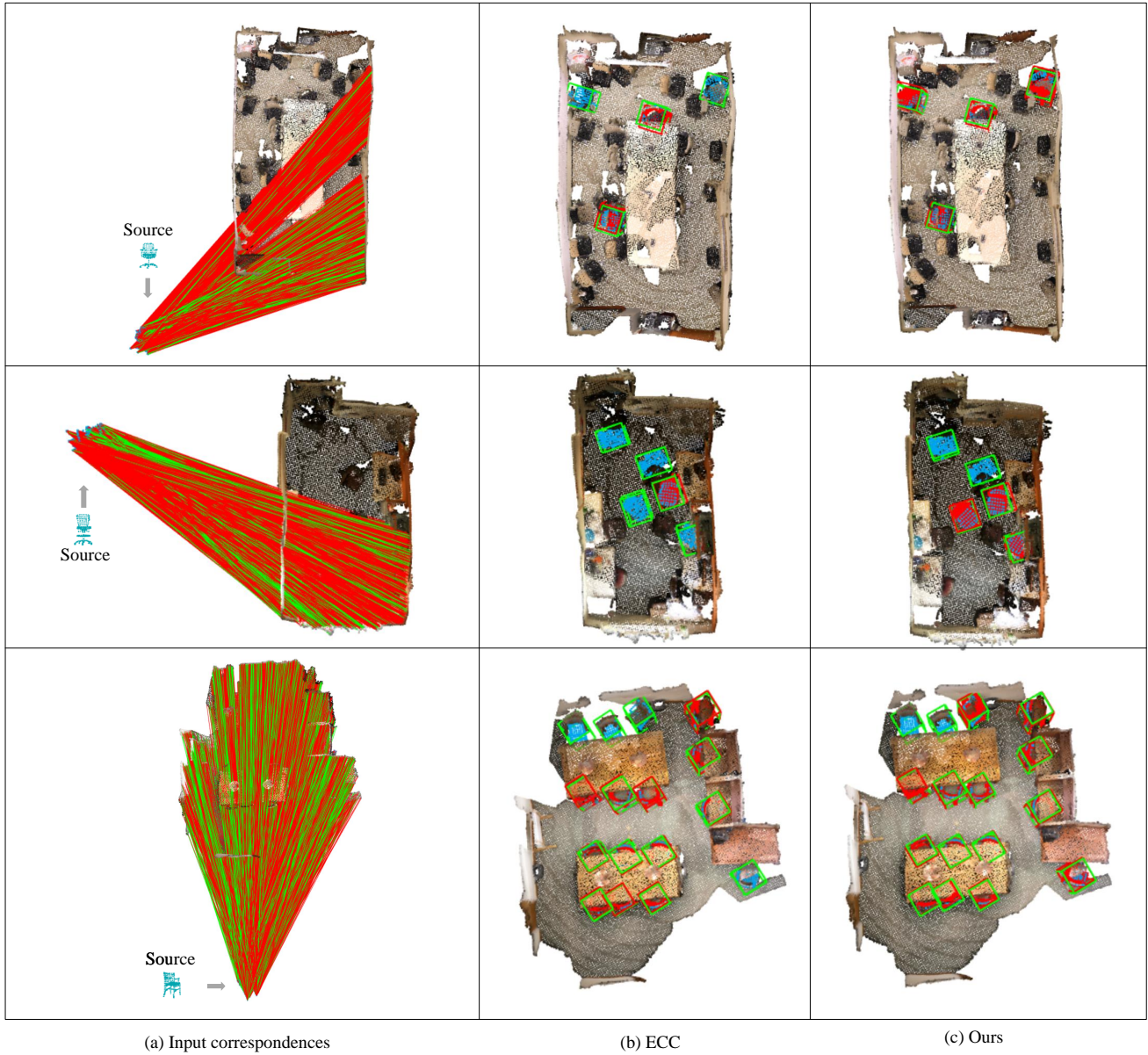


Figure 12. Visual results on the real dataset.